

Multiconfiguration microscopic study of $\alpha + {}^{14}\text{C}$ molecular states

P. Descouvemont and D. Baye

Physique Théorique et Mathématique CP 229, Université Libre de Bruxelles, B 1050 Brussels, Belgium

(Received 19 February 1985)

Antisymmetric $\alpha + {}^{14}\text{C}_{\text{g.s.}}$ and $\alpha + {}^{14}\text{C}(2_1^+)$ wave functions are used in the generator coordinate formalism to investigate molecular properties of ${}^{18}\text{O}$ states. Quadrupole moments, rms radii, and reduced α widths of these states are calculated as well as reduced $E1$ and $E2$ transition probabilities between them. A number of molecular bands are found and analyzed. The assignment of experimental states to these bands is discussed. The alternating-parity band proposed by Gai *et al.* is interpreted as a fortuitous alignment of molecular states belonging to different bands.

I. INTRODUCTION

The existence of molecular states in the ${}^{18}\text{O}$ spectrum is revealed by an enhancement of $E1$ and $E2$ transitions between these states.^{1,2} In general, molecular states in light nuclei are interpreted as arising from a dinuclear structure involving an unexcited core (${}^{14}\text{C}$ in the present case) and an α particle. The existence of such states is well established for the neighboring ${}^{16}\text{O}$ and ${}^{20}\text{Ne}$ nuclei (see Refs. 3–7 for different theoretical descriptions). More surprising is the suggestion^{1,2} that an alternating-parity molecular band is formed by some of the ${}^{18}\text{O}$ states, e.g., 0_2^+ (3.63 MeV), 1_1^- (4.46 MeV), 2_3^+ (5.26 MeV), 3_3^- (8.29 MeV), and 4_3^+ (10.26 MeV). The comparable ${}^{16}\text{O}$ and ${}^{20}\text{Ne}$ nuclei do not provide any indication on the existence of such a molecular band. On the contrary, $K^\pi=0^+$ and 0^- bands are well separated and correspond in general to rather different molecular configurations. Examples of positive- and negative-parity molecular bands are given, respectively, by the 6.05 MeV 0^+ band in ${}^{16}\text{O}$ and the 5.78 MeV 0^- band in ${}^{20}\text{Ne}$. Notice that the slopes of these ${}^{16}\text{O}$ and ${}^{20}\text{Ne}$ molecular bands are more than 30% smaller than the slope of the ${}^{18}\text{O}$ band suggested by Gai *et al.* The fact that the above-mentioned ${}^{18}\text{O}$ states, and several other ones, have a molecular parentage is well established. On the contrary, evidence for the existence of a mixed-parity band is relatively weak; it is essentially based on the fact that the five molecular states form a more-or-less straight line in a rotational diagram.

In order to investigate this problem theoretically, we have recently performed a fully microscopic calculation of the $\alpha + {}^{14}\text{C}_{\text{g.s.}}$ cluster structure.⁸ This system is studied in the framework of the generator-coordinate method (GCM),^{9,10} with an exact treatment of antisymmetrization and of good quantum numbers. The GCM antisymmetric wave functions are then employed to compute $E1$ and $E2$ reduced transition probabilities.¹¹ The microscopic results of Ref. 8 do not support the idea of a mixed-parity rotational band. For several forces, two distinct molecular bands ($K^\pi=0^+$ and 0^-) are found. Moreover, the 3^-1^- and 4^+-2^+ energy differences are always found too small to agree with the rotational constant of the band suggested in Refs. 1 and 2.

Apparently, a very different conclusion has been

reached by the Münster group¹² in a similar study. Using the orthogonality condition model¹³ (OCM) to describe the $\alpha + {}^{14}\text{C}_{\text{g.s.}}$ system, these authors confirm the existence of a mixed-parity rotational band with enhanced $E1$ transitions. Since the OCM is based on an approximation of the GCM, both approaches should however lead to concordant results. In fact, the contradiction between the conclusions of both calculations is not due to the models. In Ref. 12, Assenbaum *et al.* assume *a priori* the existence of the mixed-parity band: For each partial wave, they fit the OCM effective potential in order to reproduce the experimental energy of the molecular state. Then, they find enhanced $E1$ transitions between these states. Obviously, their study does not bring conclusive information about the very existence of the band.

In Ref. 8, we have suggested that, because of antisymmetrization, the ${}^{14}\text{C}_{\text{g.s.}}$ core could not be considered as a rigid cluster in an $\alpha + {}^{14}\text{C}_{\text{g.s.}}$ structure. Virtual excitations of the ${}^{14}\text{C}$ cluster also lead to low-lying ${}^{18}\text{O}$ states with molecular properties. This effect is well known in the ${}^{16}\text{O}$ spectrum where $\alpha + {}^{12}\text{C}^*$ configurations are essential in a realistic cluster description.^{4,7,14} The controversy about the molecular bands in the ${}^{18}\text{O}$ spectrum has thus prompted us to perform a multiconfiguration microscopic calculation of the $\alpha + {}^{14}\text{C}$ system in the GCM framework. Similar studies have already been made for the $\alpha + {}^{12}\text{C}$ and ${}^{12}\text{C} + {}^{16}\text{O}$ systems.^{14,15} For computation-time reasons, the calculation is restricted to the two configurations which are expected to be the most important, i.e., $\alpha + {}^{14}\text{C}(0^+, \text{g.s.})$ and $\alpha + {}^{14}\text{C}(2^+, 7.01 \text{ MeV})$. Indeed, as shown in Sec. II, these configurations present an important overlap because of antisymmetrization and may thus be strongly coupled. In Sec. III, the coupled-channel calculation is compared with the single-channel approach of Ref. 8 and with experimental data. Reduced $E1$ and $E2$ transition probabilities and reduced α widths are calculated. A band structure is proposed and compared with other works in Sec. IV. Concluding remarks are presented in Sec. V.

II. THEORETICAL FRAMEWORK

All the results presented in the following sections are obtained with fully antisymmetric wave functions. Formally, these wave functions resemble usual coupled-

channel wave functions but the introduction of antisymmetrization over the 18 nucleons represents a tremendous complication. The calculations are made possible by the introduction of a generator coordinate which allows one to express the wave functions as a function of Slater determinants. The occurrence of Slater determinants makes the calculation of the matrix elements systematic and well adapted to a numerical computation. Let us now present the wave functions more precisely.

First, we define the α and ${}^{14}\text{C}$ internal wave functions. Let Φ_α be a Slater determinant composed of four 0s harmonic oscillator wave functions with the different spin and isospin quantum numbers. The function Φ_α is not translation invariant, but because of the harmonic-oscillator assumption, a center-of-mass wave function can be factorized out exactly. The remaining factor ϕ_α is chosen as translation-invariant internal wave function of the α particle; it depends only on the harmonic oscillator parameter chosen. This definition of ϕ_α remains rather formal, but the explicit form of ϕ_α is never needed in actual calculations. The ${}^{14}\text{C}$ internal wave functions are readily constructed using the same technique. The ground-state internal wave function ϕ_{00} is obtained from a single Slater determinant Φ_{00} corresponding to a closed neutron p shell and to a closed proton $p_{3/2}$ subshell. The 2^+ state is obtained by exciting a $p_{3/2}$ proton into the $p_{1/2}$ subshell. The states $\Phi_{2\pm 2}$ are still described by a single Slater determinant but the states Φ_{20} and $\Phi_{2\pm 1}$ each require a linear combination of two determinants. After removing the c.m. dependence, one obtains the ${}^{14}\text{C}$ internal wave functions ϕ_{IK} . If b is the harmonic oscillator parameter, a simple calculation provides $(\frac{59}{28})^{1/2} b$ as rms radius for the ground state and $e b^2$ as the quadrupole moment for the 2^+ state. The $B(E2, 2^+ \rightarrow 0^+)$ is equal to $5/4\pi e^2 b^4$. With $b=1.7$ fm, the rms radius and $B(E2)$ are in good agreement with experimental¹⁶ values (2.59 fm—including a finite proton radius contribution—with respect to 2.56 ± 0.05 fm and $3.3 e^2 \text{ fm}^4$ with respect to $3.6 \pm 0.5 e^2 \text{ fm}^4$).

Besides its simplicity, the present jj -coupling description of the 0^+ and 2^+ states of ${}^{14}\text{C}$ offers the important advantage that it reproduces easily the energy difference between these states. The correctness of the 2^+ excitation energy is indeed essential for the study of molecular bands in order to avoid nonphysical band crossings and unrealistic partial widths.¹⁵ As shown in the Appendix, the energy difference between the 0^+ and 2^+ states depends mainly on the strength of the two-body spin-orbit interaction. For reasonable choices of the Majorana parameters m_i , the correct 2^+ excitation energy is obtained with a spin-orbit parameter¹⁷ $S_0 \approx 58 \text{ MeV fm}^5$. As for other light nuclei described in the harmonic oscillator model with the jj coupling scheme, effective two-body spin-orbit interactions have to be chosen somewhat stronger (by about 40% here) than the realistic one.¹⁷

The totally antisymmetric wave functions of the two-cluster system are defined as^{10,15}

$$\Psi^{JM\pi} = \Psi_0^{JM\pi} + \Psi_2^{JM\pi}, \quad (1)$$

with

$$\Psi_l^{JM\pi} = \sum_l \Psi_{ll}^{JM\pi} = \sum_l \mathcal{A} \phi_\alpha [\phi_l \otimes Y^l(\hat{\rho})]^{JM} g_{ll}^{J\pi}(\rho). \quad (2)$$

In Eq. (2), \mathcal{A} represents the antisymmetrization projector. The quantal relative coordinate ρ is the difference between the cluster c.m. coordinates. The sum over the orbital momentum l is restricted to even or odd values according as the parity π is positive or negative. The functions $g_{ll}^{J\pi}(\rho)$ are unknown relative wave functions to be determined from a variational principle.

Except for the occurrence of the antisymmetrizer \mathcal{A} , $\Psi^{JM\pi}$ is identical to usual coupled-channel wave functions. However, antisymmetrization introduces a major difference with coupled-channel calculations: for given J , M , and π , the functions $\Psi_0^{JM\pi}$ and $\Psi_2^{JM\pi}$ are *not* orthogonal in spite of the orthogonality between ϕ_{00} and ϕ_{2K} . Because of this overlap effect, the coupling between $\Psi_0^{JM\pi}$ and $\Psi_2^{JM\pi}$ may be rather strong. Notice that for a normalized state $\Psi^{JM\pi}$, the partial contributions $\langle \Psi_0^{JM\pi} | \Psi_0^{JM\pi} \rangle$ and $\langle \Psi_2^{JM\pi} | \Psi_2^{JM\pi} \rangle$ cannot be interpreted straightforwardly since their sum is not unity. These quantities represent probabilities of a given configuration only when $\langle \Psi_0^{JM\pi} | \Psi_2^{JM\pi} \rangle$ is much smaller than unity.

In the GCM formalism, the wave functions are expressed as a function of Slater determinants. For this purpose, it is convenient to choose a common value for the harmonic oscillator parameters of both clusters. This choice, which leads to a somewhat too large α -particle radius, represents an important economy of computation time. Let us consider two harmonic oscillator wells located at a distance R from each other. The GCM basis functions^{9,10} are defined as

$$\Phi_{IK}^{JM\pi}(R) = \sum_{K=-I}^I (II0K | JK) P_{KM}^J \Phi_{IK}^{\alpha+{}^{14}\text{C}}(R\hat{z}), \quad (3)$$

with

$$\Phi_{IK}^{\alpha+{}^{14}\text{C}}(\mathbf{R}) = \mathcal{A} \Phi_\alpha(-\frac{14}{18}\mathbf{R}) \Phi_{IK}(\frac{4}{18}\mathbf{R}). \quad (4)$$

The antisymmetric product in (4) is a linear combination of at most two Slater determinants. Its component with angular momentum J and projection M is projected out by operator P_{KM}^J in (3). The correct relative orbital momentum l and parity are then obtained through angular momentum coupling. The distance R is taken as the generator coordinate and the wave functions $\Psi_{ll}^{JM\pi}$ of Eq. (2) are approximated by

$$\Psi_{ll}^{JM\pi} = \sum_n \int_{lln}^{J\pi} \Phi_{ll}^{JM\pi}(R_n), \quad (5)$$

i.e., by an expression linearly combining basis functions taken at different values of the generator coordinate. Since $\Phi_{IK}^{\alpha+{}^{14}\text{C}}$ is a combination of Slater determinants, all the calculations of matrix elements are systematic. For bound states and narrow resonances, the unknown coefficients $\int_{lln}^{J\pi}$ in (5) are determined by applying the variational principle. As shown in Ref. 18, this bound-state approximation accurately yields transition probabilities and α widths for resonances whose widths are smaller than a few hundred keV. For broader resonances, scattering techniques^{10,11} have to be applied.

In order to have a deeper insight into the configurations that we have selected, let us consider the properties of the GCM basis functions for small values of the generator coordinate R . Obviously, when R tends towards zero, the Slater determinants in (4) vanish because they have identical columns. More precisely, one has

$$\Phi_{IK}^{\alpha+^{14}\text{C}} \underset{R \rightarrow 0}{\sim} R^6 \chi_{2p} + \dots \quad (6)$$

The shell-model state χ_{2p} is composed of a closed ^{16}O shell and two neutrons with opposite spins in the (002) Cartesian harmonic oscillator state. Except for an irrelevant normalization factor, this state is independent of I and K . The different configurations in our calculation have thus the *same limit* for vanishing distances R . This property explains that the $\alpha + ^{14}\text{C}(2^+)$ configuration is the most strongly coupled with the $\alpha + ^{14}\text{C}(0^+)$ configuration. On the other hand, the 2p shell model space contained in our model is not complete. Its extension would require the introduction of additional molecular configurations like $\alpha + ^{14}\text{C}(1^-)$ and $\alpha + ^{14}\text{C}(3^-)$. Such a multiconfiguration calculation is, however, presently too complicated.

For projected basis states, Eq. (6) can be generalized as

$$\Phi_{II}^{JM\pi} \underset{R \rightarrow 0}{\sim} R^{2m_{II}^{J\pi}+l} \chi^{JM\pi} + \dots \quad (7)$$

In this expression, $m_{II}^{J\pi}$ is the number of so-called forbidden or redundant states. The forbidden states are functions $g_{II}^{J\pi}$ different from zero for which an antisymmetric wave function $\Psi_{II}^{JM\pi}$ defined by Eq. (2) vanishes.^{9,17} The numbers $m_{II}^{J\pi}$ calculated as explained in Ref. 17 are given in Table I. The shell model wave functions $\chi^{JM\pi}$ correspond to $2m_{II}^{J\pi}+l-6$ harmonic oscillator quanta of excitation with respect to the 2p configurations. As a consequence, different states corresponding to the same power $2m_{II}^{J\pi}+l$ are in general obtained from the same intrinsic state and will exhibit band properties as exemplified in Sec. III.

III. RESULTS

A. Bound-state and resonance properties

The microscopic calculation is performed with Volkov¹⁹ V_2 plus spin-orbit¹⁷ and exact Coulomb interactions. The harmonic oscillator parameter is chosen as 1.7 fm. In order to reproduce correctly the experimental²⁰ energy of the 0_2^+ and 1_1^- states of ^{18}O , we have used a slightly different Majorana parameter for both parities ($m=0.618$ for positive parity and $m=0.636$ for negative parity). The spin-orbit amplitude is determined by requiring that the excitation energy of the $^{14}\text{C}(2^+)$ is exactly reproduced (see the Appendix). This condition yields $S_0=57.91$ MeV fm⁵ for positive parity and $S_0=58.25$ MeV fm⁵ for negative parity.

Notice that we have used the few available parameters to fit the quantities that we consider as important for a band-structure study, i.e., the properties of the ^{14}C cluster, the energy separation between the channels, and the location of the band heads. Because of the equal-oscillator-parameter assumption, the α -particle radius is overestimated. Moreover, the internal energies of the α and ^{14}C

TABLE I. Numbers of forbidden states.

J^π	II				J^π	II	
	$J,0$	$J-2,2$	$J,2$	$J+2,2$		$J-1,2$	$J+1,2$
0^+	3			2	0^-		
2^+	2	3	2	1	2^-	3	2
4^+	1	2	1	0	4^-	2	1
6^+	1	2	1	0	6^-	1	0
8^+	0	1	0	0	8^-	0	0
$\geq 10^+$	0	0	0	0	$\geq 10^-$	0	0
1^-	3		3	2	1^+		3
3^-	2	3	2	1	3^+	3	2
5^-	1	2	1	0	5^+	2	1
7^-	0	1	0	0	7^+	1	0
9^-	0	1	0	0	9^+	0	0
$\geq 11^-$	0	0	0	0	$\geq 11^+$	0	0

clusters are not minimized with respect to this parameter.

In Fig. 1(a), we display the location of the states obtained without coupling between the $I=0$ and $I=2$ configurations, i.e., by using only one component of the wave function (1). The energies corresponding to $\Psi_0^{JM\pi}$ are plotted as open circles. They are very similar to those obtained in Ref. 8 where a slightly different nuclear interaction was used. The ground-state band is not presented in Fig. 1. The states of this band are located 10.2(0_1^+), 9.4(2_1^+), and 8.3(4_1^+) MeV below the $\alpha + ^{14}\text{C}$ threshold when only the $\alpha + ^{14}\text{C}(0^+)$ configuration is taken into account. As it was found in Ref. 8, the binding energies of these states are too large. This effect is partly due to the fact that the α and ^{14}C binding energies are underestimated. The solid circles and squares (natural and non-natural-parity states, respectively) represent the energies corresponding to the wave function $\Psi_2^{JM\pi}$ solely. The ground-state band obtained with $\Psi_2^{JM\pi}$ (-10.5 , -9.7 , -8.5 MeV) is slightly lower than with $\Psi_0^{JM\pi}$. The similarity of the descriptions of the ground-state band with $\Psi_0^{JM\pi}$ and $\Psi_2^{JM\pi}$ is a consequence of the fact that these

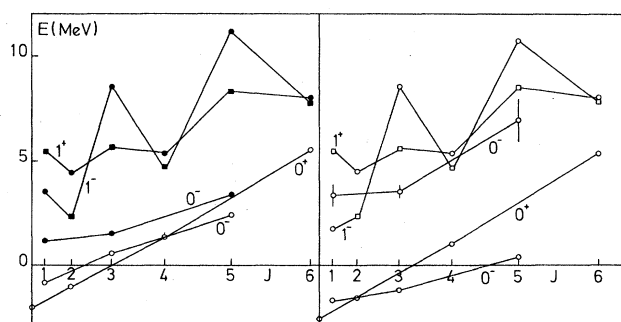


FIG. 1. (a) Bound-state and resonance energies with respect to the $\alpha + ^{14}\text{C}$ threshold obtained with a single configuration. The open circles represent the states obtained with $\Psi_0^{JM\pi}$. The full circles and squares represent the natural and non-natural-parity states obtained with $\Psi_2^{JM\pi}$. (b) The same as Fig. 1(a) with the two configurations $\Psi_0^{JM\pi}$ and $\Psi_2^{JM\pi}$. The vertical bars indicate the width of the resonances.

TABLE II. Positive-parity states. E_x^{th} is obtained by adding 6.23 MeV to the theoretical c.m. energy E^{th} defined with respect to the $\alpha + {}^{14}\text{C}(0^+)$ threshold. The dimensionless reduced α widths are calculated with a channel radius of 6 fm.

J^π	E^{th} (MeV)	E_x^{th} (MeV)	E_x^{exp} (MeV)	Q_0 ($e \text{ fm}^2$)	θ_0^2 (%)	θ_2^2 (%)	d (fm)
0_1^+	-11.0	-4.8	0		0.24	0.05	3.03
2_1^+	-10.1	-3.9	1.98	6	0.15	0.04	2.96
4_1^+	-8.7	-2.5	3.55	3	0.03	0.01	2.80
0_2^+	-2.6	3.6	3.63		20.8	0.14	4.38
2_3^+	-1.5	4.7	5.26	58	19.5	0.10	4.37
4_2^+	1.1	7.3	7.12	57	17.3	0.03	4.34
6_1^+	5.4	11.6	11.69	57	14.6	0.11	4.34
$8_{(1)}^+$	11.5	17.7		46	8.2	1.2	4.04
$1_{(1)}^+$	5.5	11.7		48		20.7	4.49
2_4^+	4.5	10.7	8.22	1	0.5	21.1	4.55
$3_{(1)}^+$	5.7	12.0		16		21.8	4.50
4_3^+	5.4	11.6	10.26	73	0.8	16.1	5.11
$5_{(1)}^+$	8.5	14.7		47		20.0	4.46
6_2^+	8.1	14.3	12.53	77	2.0	13.4	5.19

wave functions become proportional at small interdistances (see Sec. II). The 0^- band is close to, but distinct from, the 0^- band obtained in the elastic-channel calculation. Both descriptions of the negative-parity band are thus not expected to be equivalent. Because of the nonorthogonality of $\Psi_0^{JM\pi}$ and $\Psi_2^{JM\pi}$, the proximity of these bands in the uncoupled calculation can yield two 0^- bands with strongly different properties in the coupled-channel study. Several other bands corresponding to constant values of $2m_{II}^{J\pi} + l$ are expected from Table I, but we restrict our study to the most important of them.

The spectrum obtained by mixing the $\alpha + {}^{14}\text{C}(0^+)$ and $\alpha + {}^{14}\text{C}(2^+)$ configurations is depicted in Fig. 1(b), and we present in Tables II and III the energies, quadrupole moments, reduced alpha widths, and mean distances between the clusters. The energies E_x^{th} are obtained by adding the experimental $\alpha + {}^{14}\text{C}(0^+)$ threshold energy to the theoretical c.m. energy:

$$E_x^{\text{th}} = E^{\text{th}} + 6.23 \text{ MeV} . \quad (8)$$

This definition is useful for the sake of comparison with the experimental data; however, it leads to a negative exci-

TABLE III. Negative-parity states. (See caption to Table II.)

J^π	E^{th} (MeV)	E_x^{th} (MeV)	E_x^{exp} (MeV)	Q_0 ($e \text{ fm}^2$)	θ_0^2 (%)	θ_2^2 (%)	d (fm)
1_1^-	-1.7	4.5	4.46	35	12.5	0.6	4.13
3_1^-	-1.2	5.0	5.10	29	4.9	0.8	3.75
5_1^-	0.4	6.6	8.13	23	1.5	0.4	3.40
$7_{(1)}^-$	2.9	9.1		18	0.2	0.1	3.06
1_3^-	3.4	9.6	7.62	~ 120	36	1.4	~ 7
3_3^-	3.6	9.8	8.29	~ 110	39	1.1	~ 6
5_2^-	6.9	13.1	11.62	~ 180	60	1.4	~ 8
1_2^-	1.8	8.0	6.20	-27	5	3.1	4.42
2_2^-	2.4	8.6	7.77	44		3.4	3.64
$3_{(4)}^-$	8.6	14.8		39	4	2.9	5.66
$4_{(1)}^-$	4.7	10.9		36		2.1	3.46
$5_{(3)}^-$	10.8	17.0		41	6	2.8	4.03
$6_{(1)}^-$	7.9	14.1		29		0.6	3.15

tation energy of the GCM ground-state band. The quadrupole moments in a band K^π are presented in the form of intrinsic quadrupole moments Q_0 defined by²¹

$$Q = Q_0 [3K^2 - J(J+1)] / (J+1)(2J+3), \quad (9)$$

where Q is the microscopic quadrupole moment.¹¹ The constancy of the Q_0 values in a band indicates the rotational character of this band. The dimensionless reduced α widths in the $I=0$ and $I=2$ channels are labeled by θ_0^2 and θ_2^2 , respectively. By extending Eq. (4) of Ref. 18, one gets

$$\theta_J^2 = (256\pi^5 a^3 / 3) \sum_l |g_{lI}^{J\pi}(a)|^2 / (2l+1), \quad (10)$$

where a is the channel radius; this radius must be chosen large enough (6 fm in the present calculation) so that the antisymmetrization operator in (2) is negligible. For not too broad states (whose total α width is lower than about 0.5 MeV), this bound-state approximation leads to θ_J^2 values close to those obtained from a phase-shift analysis. For broad resonances a fully dynamical calculation has been performed. Finally, the mean distance d is related to the mean square radius $\langle r^2 \rangle$ by

$$d^2 = \left(\frac{18}{56}\right) (18\langle r^2 \rangle - 4\langle r^2 \rangle_\alpha - 14\langle r^2 \rangle_{^{14}\text{C}}), \quad (11)$$

where $\langle r^2 \rangle_\alpha$ and $\langle r^2 \rangle_{^{14}\text{C}}$ are the mean square radii of α and ^{14}C , respectively. For the states belonging to a rotational band, the d values are expected to be nearly J independent.

The positive-parity bands are weakly affected by the coupling, the 0^+ and 1^+ bands being obtained mainly from one $\alpha + ^{14}\text{C}$ configuration. As expected from the variational principle, the ground-state band is slightly pushed down with respect to the single-configuration calculations (-11.0 , -10.1 , -8.7 MeV), but the excited configuration does not modify significantly the properties of these states (see Ref. 8). The members of the ground-state band are close to a shell-model structure, and the $2p$ configuration towards which the GCM wave function tends at small interdistances is not flexible enough to provide a more realistic description of the shell-model states.

1. The 0_2^+ band

This band presents a marked rotational nature in the $\alpha + ^{14}\text{C}(0^+)$ channel. The important values of Q_0 and d indicate a molecular shape of these states. The $\alpha + ^{14}\text{C}(0^+)$ structure of this band is confirmed by the large dimensionless α widths in the elastic channel. On the contrary, the θ_2^2 values are significantly smaller. The energy locations obtained in our theoretical calculation suggest to identify the states of the 0_2^+ band with the experimental²⁰ 0_2^+ , 2_3^+ , 4_2^+ , and 6_1^+ states, whose energies nicely agree with our results. The assignment of these experimental states to a rotational band has already been proposed by Buck *et al.*²² in a local-potential model calculation. Moreover, the same conclusion has been drawn in the experimental analysis of Cunsolo *et al.*²³ The slight disagreement observed for the 2_3^+ state is explained by the absence in our calculation of the 2_2^+ state at

$E_x = 3.92$ MeV. Our theoretical investigation predicts an 8^+ resonance in the molecular band at $E_x \approx 18$ MeV with a width of about 0.1 MeV. Let us notice the similarity between the 0_2^+ band in ^{18}O and the 0_1^+ band in the ^{16}O nucleus. By fitting the experimental energies of these bands (from $J^\pi = 0^+$ up to $J^\pi = 6^+$) to a rotational law, one finds 5.9 and 5.3 fm, respectively, as the distances between the $\alpha + ^{14}\text{C}$ and $\alpha + ^{12}\text{C}$ clusters. Moreover, the values of the quadrupole moments and of the rms radii obtained in the present study are very similar to those calculated with the same method for the 0_1^+ band in the $\alpha + ^{12}\text{C}$ system.²⁴

2. The 1^+ band

The states belonging to this band have mainly an $\alpha + ^{14}\text{C}(2^+)$ structure, and the coupling with the elastic channel does not significantly affect their energy location [compare Figs. 1(a) and (b)]. Because of their large reduced width in the excited channel, these states can be considered as molecular $\alpha + ^{14}\text{C}(2^+)$ states. This interpretation is supported by the large distances and intrinsic quadrupole moments of most of the states. Let us point out that the constancy of the Q_0 values is not fully realized because of the presence of many other states in the vicinity of the 1^+ band. This is especially the case for the 2_4^+ and $3_{(1)}^+$ states. However, the similarity of the θ_2^2 and d values gives some confidence in the assignment of the states belonging to this band. There are no experimental candidates for the non-natural-parity states. However, the theoretical 2_4^+ (10.7 MeV) state could correspond to the experimental 2_4^+ (8.22 MeV) level, which presents²⁰ a very small α width ($\theta_0^2 = 0.6\%$), in nice agreement with our calculation. The overestimation of the energy in the GCM study can be explained by the lack of other configurations [e.g., the $\alpha + ^{14}\text{C}(3^-)$ and $\alpha + ^{14}\text{C}(1^-)$ configurations] whose effect on the energy locations could be non-negligible. If one keeps in mind this overestimation of about 2 MeV, the 4_3^+ and 6_2^+ states can be considered as the experimental 4_3^+ (10.30 MeV) and 6_2^+ (12.53 MeV) states. For the 4_3^+ state, the disagreement between the theoretical reduced α width ($\theta_0^2 = 0.8\%$) and the experimental¹ one ($\theta_0^2 \approx 15\%$) arises from too weak a coupling with the molecular 4_2^+ resonance in the GCM calculation; this yields too small an $\alpha + ^{14}\text{C}(0^+)$ component in the GCM 4_3^+ wave function. Notice that similar results have been obtained by Sakuda *et al.*²⁵ ($\theta_0^2 = 0.5\%$ for the 4_3^+ state and $\theta_0^2 = 4.5\%$ for the 6_2^+ state). Besides, because of its high excitation energy, the 4_3^+ state is most likely affected by the neutron channel.²⁶

It is interesting to notice that, even below the inelastic threshold, the $\alpha + ^{14}\text{C}(2^+)$ channel may strongly affect the elastic phase shifts. To illustrate this point, we compare in Fig. 2(a) the elastic phase shifts of the 4^+ partial wave obtained in the single-channel calculation (dashed line), and in the multichannel one (solid line). Obviously, the effect of the $\alpha + ^{14}\text{C}(2^+)$ configuration is the introduction of a narrow resonance at $E_{\text{c.m.}} = 5.4$ MeV, which is not apparent in the single-channel study. The resonance corresponds to the formation of a bound $\alpha + ^{14}\text{C}(2^+)$ system; however, this configuration is not stable with respect to the elastic channel, and hence may decay to an unbound $\alpha + ^{14}\text{C}(0^+)$ system. This effect is easily visualized

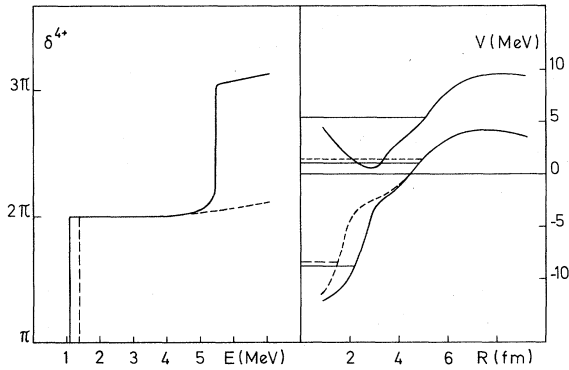


FIG. 2. (a) Elastic phase shift of the 4^+ partial wave in the single-channel (dashed line) and in the multichannel (solid line) calculations as a function of the c.m. energy. (b) Locations of the states obtained in the GCM calculation (horizontal bars). The quasideagonal energy curves relative to the 4^+ partial wave are plotted as solid lines for the multichannel calculation and as a dashed line for the single-channel calculation.

in Fig. 2(b) where we have plotted the elastic and first inelastic quasideagonal energy curves.¹⁵ The energy curves represent the expectation value of the Hamiltonian at a given cluster interdistance; they are straightforwardly deduced from the overlap and Hamiltonian kernels. For a light system, such as $\alpha + {}^{14}\text{C}$, the energy curves should not be strictly considered as nucleus-nucleus potentials.²⁷ Nevertheless, they bring useful information about the nature of the considered states. We have represented by horizontal lines the energies of the different 4^+ states. The 4_1^+ bound state is not affected much by the excited channel. However, the 4_2^+ resonance lies above the bottom of the first $\alpha + {}^{14}\text{C}(2^+)$ well, which leads to a decrease of its elastic component. This reduction is revealed by the θ_0^2 and d values which are lowered with respect to the single-channel calculation⁸ ($\theta_0^2 = 28\%$ and $d = 5.09$ fm). Besides, from the energy-curve picture, the 4_3^+ state can be interpreted as a bound $\alpha + {}^{14}\text{C}(2^+)$ system.

3. The 0_1^- band

The comparison of Figs. 1(a) and (b) shows that this band is rather strongly affected by the $\alpha + {}^{14}\text{C}(2^+)$ configuration. With respect to the single-channel investigation,⁸ the present study leads to a less pronounced cluster structure and hence to less pronounced molecular properties: the reduced α widths are lowered by more than a factor of 2, and the distances between the α and ${}^{14}\text{C}$ clusters are reduced by about 1 fm. Notice that this effect becomes more and more important with increasing values of J .

In our previous study we assigned the theoretical 3^- state to the experimental 3_2^- (6.40 MeV) state, as suggested by the comparison between the theoretical 1^- - 3^- and experimental 1_1^- - 3_2^- energy gaps. However, our multichannel calculation exhibits a very small energy difference between the lowest 1^- and 3^- states, which leads us to assign the theoretical 3^- (5.0 MeV) to the experimental 3_1^- (5.10 MeV) state. A reasonable experimental candi-

date for $J^\pi = 5^-$ is the 5_1^- (8.13 MeV) state, whose α width should be very small; our investigation also predicts a narrow ($\Gamma_\alpha < 1$ eV) 7^- resonance around $E_x = 10$ MeV.

4. The 0_2^- band

This band contains broad resonances, located above the Coulomb barrier of the elastic channel, and resulting from the coupling of the $\alpha + {}^{14}\text{C}(0^+)$ and $\alpha + {}^{14}\text{C}(2^+)$ configurations. The large reduced α widths correspond to total widths equal to 1 MeV (1_3^-), 0.5 MeV (3_3^-), and 2 MeV (5_2^-). Since the bound-state approximation is not accurate for such broad states, the Q_0 and d values are indicative only. They show a marked cluster structure of the 1_3^- , 3_3^- , and 5_2^- states. The 1_3^- state is expected to be the most influenced by the inelastic channel, since an inversion between two 1^- states occurs when both channels are coupled [compare Figs. 1(a) and (b)].

We illustrate the influence of the $\alpha + {}^{14}\text{C}(2^+)$ configuration on this band by comparing in Fig. 3(a) the 3^- phase shifts obtained with the single-channel (dashed line) and multichannel (solid line) calculations. The effect of the inelastic channel is to lower the energy of a small bump present in the single-channel calculation, yielding a more apparent resonance at $E_{c.m.} \approx 3.6$ MeV. The energy curves displayed in Fig. 3(b) support this interpretation: The 3_3^- resonance is located just above the well of the first inelastic energy curve, but its component in this channel is weak. The overlap between Ψ_0^{3M-} and Ψ_2^{3M-} being small ($\approx 10^{-3}$), the partial contribution $\langle \Psi_0^{3M-} | \Psi_0^{3M-} \rangle = 0.8$ can be interpreted as a probability. Hence the influence of the $\alpha + {}^{14}\text{C}(2^+)$ configuration is mainly restricted to a decrease of the excitation energy.

Because of their large α widths, the theoretical 1_3^- (9.6 MeV) and 3_3^- (9.8 MeV) states can be considered as good candidates for the experimental 1_3^- (7.62 MeV) and 3_3^- (8.29 MeV) states, which are known to have an important molecular parentage²⁰ [$\theta_0^2(1_3^-) < 6\%$ and $\theta_0^2(3_3^-) = 15 \pm 2\%$]. It must be emphasized that, although these states have large components in the $\alpha + {}^{14}\text{C}(0^+)$ channel, our calculation shows that they cannot be described in a single-channel picture.

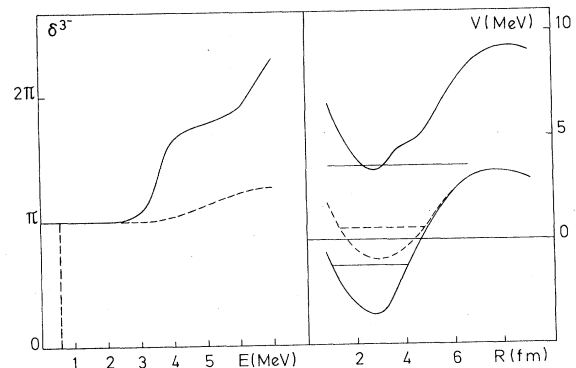


FIG. 3. Same as Fig. 2 for the 3^- partial wave.

5. The 1^- band

Although the states 1_2^- , 2_2^- , $3_{(4)}^-$, $4_{(1)}^-$, $5_{(3)}^-$, and $6_{(1)}^-$ do not follow a rotational sequence (see Fig. 1), their properties are qualitatively similar, and hence these states can be considered as forming a band. Except for the 1_2^- state, all the states of this band are weakly modified when both channels are coupled [compare Figs. 1(a) and (b)]. The intrinsic quadrupole moments are nearly constant, except for the 1_2^- state, whose properties are strongly affected by other 1^- resonances in its vicinity. The coupling with neighboring states also explains the important deviations of the $3_{(4)}^-$ and $5_{(3)}^-$ states from the pure rotational law. The mean distances d indicate a marked molecular structure of the natural-parity states, while the non-natural-parity states are closer to shell-model configurations. From energy and electric-transition-amplitude considerations (see below), we propose the experimental 1_2^- (6.20 MeV) and 2_2^- (7.77 MeV) states as candidates for the 1_2^- (8.0 MeV) and 2_2^- (8.6 MeV) states obtained in the present study.

B. $E1$ transitions

The $E1$ transitions (see Ref. 11 for details on the calculation) are displayed in Table IV, and compared with the results of the single-channel calculation,⁸ and the experimental data of Refs. 1 and 20. The transition amplitudes between the 0_1^- and 0_1^+ bands are not significantly modified in the multichannel study. They are much too large with respect to the experimental values. The disagreement results from the lack of flexibility of the 2p shell-model component in the GCM wave function; this problem is not solved by the introduction of the $\alpha + {}^{14}\text{C}(2^+)$ configuration. On the contrary, the $E1$ transition amplitudes between the molecular 0_1^- and 0_2^+ bands are

markedly reduced with respect to the single-channel study, in better agreement with the experimental data. This decrease arises from the reduction of the $\alpha + {}^{14}\text{C}(0^+)$ molecular components in these bands, and hence of the overlap between them. It is likely that the introduction of the $\alpha + {}^{14}\text{C}(3^-)$ and $\alpha + {}^{14}\text{C}(1^-)$ configurations would still reduce the $E1$ matrix elements and lead to a good agreement with experiment.

We illustrate the $E1$ transitions between other bands by a few typical examples. The transitions from the 3_3^- resonance are stronger towards the 0_2^+ band than towards the 0_1^+ band, revealing similar molecular properties of the 3_3^- resonance and of the members of the 0_2^+ band. Although the overall agreement with experiment is not good, there is experimental evidence for this enhancement. The same phenomenon occurs for the 1^- band, the agreement with experiment being rather good for the $1_2^- \rightarrow 0_1^+$ and $1_2^- \rightarrow 2_3^+$ transitions. The large experimental value for the $1_2^- \rightarrow 2_3^+$ transition amplitude is confirmed by our theoretical approach, indicating that, as suggested in Ref. 1, the molecular properties in ${}^{18}\text{O}$ are shared by several states. From this conclusion, the very weak experimental transition amplitudes between the 1_2^- and 0_2^+ states, which are both shown to have an important molecular parentage, is unexplainable by our model.

We also present in Table IV the $E1$ transitions from the 2_4^+ and 4_3^+ states, which belong to the 1^+ band. The comparison with the available experimental data shows that the GCM values are too large. This is probably due, as for the transitions between the 0_1^- and 0_2^+ bands, to an excess of molecular components in the theoretical wave functions. A striking fact is the enhancement of the $4_3^+ \rightarrow 3_3^-$ transition amplitude, indicating similar cluster structure for both resonances. However, the small energy difference between them reduces the γ width of the transition. With the theoretical values, the branching ratio of

TABLE IV. Reduced $E1$ transitions probabilities (in 10^{-3} W.u.).

$J_i^{\pi_i}$	$J_f^{\pi_f}$	Theory		Expt.		$J_i^{\pi_i}$	$J_f^{\pi_f}$	Theory	Expt.
		a	b	Ref. 1	Ref. 20				
1_1^-	0_1^+	28	24	$< 10^{-4}$		1_2^-	0_1^+	1.1	1
1_1^-	2_1^+	40	32	0.5	0.38 ± 0.08	1_2^-	2_1^+	1.8	
3_1^-	2_1^+	23	26		0.57 ± 0.23	1_2^-	0_2^+	29	0.8
3_1^-	4_1^+	11	10			1_2^-	2_3^+	52	22
5_1^-	4_1^+	8	15						
1_1^-	0_2^+	63	130	28	28 ± 6	2_4^+	1_1^-	13	4
2_3^+	1_1^-	84	160	9	8.1 ± 1.0	2_4^+	3_1^-	30	4
3_1^-	2_3^+	52	140			2_4^+	1_2^-	38	
4_2^+	3_1^-	74	170			2_4^+	3_3^-	38	
3_3^-	2_1^+	1.4		< 0.01		4_3^+	3_1^-	22	
3_3^-	4_1^+	0.5		6		4_3^+	5_1^-	21	
3_3^-	2_3^+	94		22		4_3^+	3_3^-	116	
3_3^-	4_2^+	111							

^aMulticonfiguration calculation.

^bSingle-configuration calculation (Ref. 8) (with $\Psi_0^{JM\pi}$ only).

TABLE V. Reduced $E2$ transitions probabilities (in W.u.) between positive-parity states. (See caption to Table IV.)

$J_i^{\pi_i}$	$J_f^{\pi_f}$	Theory		Expt.		$J_i^{\pi_i}$	$J_f^{\pi_f}$	Theory
		a	b	Ref. 1	Ref. 20			
2_1^+	0_1^+	2.9	2.4	3	3.3	2_4^+	$1_{(1)}^+$	18
4_1^+	2_1^+	2.1	1.5	4	1.2	2_4^+	0_1^+	0.06
						2_4^+	2_1^+	0.18
2_3^+	0_2^+	24	29	27	20 ± 10	2_4^+	4_1^+	0.16
4_2^+	2_3^+	32	43	< 11		2_4^+	0_2^+	2.0
6_1^+	4_2^+	30	58			2_4^+	2_3^+	0.20
						2_4^+	4_2^+	0.03
2_3^+	0_1^+	1.6	5.0	2	2.0 ± 0.1	4_3^+	2_4^+	29
0_2^+	2_1^+	4.3	13.8	20	17 ± 2	4_3^+	$3_{(1)}^+$	13
2_3^+	2_1^+	1.5	4.6		1.3 ± 0.5	4_3^+	2_1^+	0.14
4_2^+	2_1^+	2.3	6.2	3		4_3^+	4_1^+	0.09
2_3^+	4_1^+	0.7	1.9	25	19 ± 8	4_3^+	2_3^+	5.2
4_2^+	4_1^+	0.6	1.4			4_3^+	4_2^+	1.4
6_1^+	4_1^+	1.3	2.2					

the 4_3^+ state is about 6% towards the 3_3^- resonance. Nevertheless, this example shows that two states may have similar molecular parentage, although they are members of different bands.

C. $E2$ transitions

We present in Tables V and VI $E2$ transitions between positive and negative parity, respectively. According to our previous single-channel investigation,⁸ an effective charge $\delta e = 0.3e$ is used for $E2$ transitions involving states of the ground-state band. The effective charge corrects for missing core polarization effects, which are important in the shell-model-type of states. For molecular states, the deformation is represented by the cluster structure of the system and effective charges should not be necessary. The $E2$ transition amplitudes provide a confirmation of the assignment of the states into bands since in a rotational band, a nearly J -independent intrinsic quadrupole moment can be deduced from the $B(E2)$ values.²¹

The $E2$ transition amplitudes inside the 0_1^+ and 0_2^+ bands are not significantly modified in the multichannel approach. On the contrary, for the same reasons as stated above (i.e., a reduction of the molecular component in the GCM wave functions), the transition amplitudes between these bands are reduced in the present study, leading to a better agreement with the experiment. Similar results

have been obtained by Sakuda *et al.*,²⁵ who use an effective charge $0.2e$ for cluster states and $0.5e$ for 2p states. Notice that almost all the transitions involving the 0_1^+ or 0_2^+ band are obviously improved in the multichannel cal-

TABLE VI. Reduced $E2$ transitions probabilities (in W.u.) between negative-parity states. (See caption to Table IV.)

$J_i^{\pi_i}$	$J_f^{\pi_f}$	Theory		Exp Ref. 1
		a	b	
3_1^-	1_1^-	11	26	
5_1^-	3_1^-	8	15	24
7_1^-	5_1^-	4	4	
3_3^-	1_1^-	13		15
3_3^-	3_1^-	4		
2_2^-	1_1^-	2		
2_2^-	3_1^-	5		
2_2^-	3_3^-	2		
2_2^-	1_2^-	7		
$3_{(4)}^-$	1_1^-	0.03		
$3_{(4)}^-$	3_1^-	0.7		
$3_{(4)}^-$	3_3^-	0.07		
$3_{(4)}^-$	1_2^-	1		
$3_{(4)}^-$	2_2^-	0.7		

ulation. However, the large experimental $B(E2)$ values for $0_2^+ \rightarrow 2_1^+$ and $2_3^+ \rightarrow 4_1^+$ remain inexplicable. The in-band transitions in the 1^+ band are much stronger than the transitions from the 1^+ to the 0_1^+ or 0_2^+ band. This is easily explained by the weak mixing between these bands.

The situation is rather different for the negative-parity states. The lowest 0^- band being strongly influenced by the $\alpha + {}^{14}\text{C}(2^+)$ configuration, the $E2$ transition amplitudes in this band are significantly reduced in the multichannel calculation with respect to the single-channel study. If one considers the experimental value 24 W.u. for the $5_1^- \rightarrow 3_1^-$ transition, this reduction seems even too important. An experimental determination of the $B(E2, 3_1^- \rightarrow 1_1^-)$ would be useful for the study of the 0_1^- band.

The similarity of the $3_1^- \rightarrow 1_1^-$ and $3_3^- \rightarrow 1_1^-$ transitions (the latter being in good agreement with the experimental value) shows once more that molecular properties can be shared by several states. The transitions from the 1^- band do not present a selective behavior, as was the case for the 1^+ band. This fact confirms the complexity of the negative-parity states, and the mixing of their molecular properties.

IV. DISCUSSION

The determination of the precise nature of the ${}^{18}\text{O}$ states is a long-standing problem to which many papers have been devoted (see, e.g., references in Refs. 25 and 28). The interpretation of some of these states in terms of nuclear molecules²² and the search for molecular bands¹ are more recent. A molecularlike band had, however, already been proposed by Morgan *et al.*²⁶ in 1970. These authors noticed that the well-deformed 0_2^+ (3.63 MeV) and 2_3^+ (5.25 MeV) states form an apparent rotational band with the 4_3^+ (10.29 MeV) resonance observed in α scattering on ${}^{14}\text{C}$. These states are nothing but the positive-parity states of the dipole molecular band proposed by Gai *et al.*^{1,2} Alignment reasons also led Morgan *et al.* to attribute the 4_2^+ (7.10 MeV) state to a band containing the ground and 2_1^+ states.

These attributions of the 4_2^+ and 4_3^+ states, as well as the attribution of the 3_3^- state,^{1,2} are in contradiction with several experimental analyses (see, e.g., Ref. 23) and with most of the theoretical studies. For example, Lawson *et al.*²⁸ study the ${}^{18}\text{O}$ nucleus with a model in which the full 2p shell-model space is mixed with deformed collective states. The contributions of the collective states are found dominant in the 0_2^+ , 2_3^+ , and 4_2^+ states. Although the collective states are interpreted in Ref. 28 as projections of a deformed Nilsson state, and not of an $\alpha + {}^{14}\text{C}$ molecule, these results are in excellent qualitative agreement with ours. An explicitly molecular model has been studied by Buck *et al.*²² The ${}^{18}\text{O}$ nucleus is described as an $\alpha + {}^{14}\text{C}_{\text{g.s.}}$ structure in the simple cluster model of Ref. 3. The results suggest a 0^+ molecular band composed of the 0_2^+ , 2_3^+ , 4_2^+ , and 6_1^+ states. All the states of this band have a dominant $\alpha + {}^{14}\text{C}_{\text{g.s.}}$ parentage in our calculation. This agreement is natural since the model of Buck *et al.* can also be derived as an approximation of the GCM. This band is also confirmed by the microscopic analysis

of Sakuda and co-workers.²⁵ In this microscopic model, all the 2p or 3p-1h shell-model states are mixed with rigid α -cluster configurations which simulate 4p-2h and higher excited configurations. These α -cluster states correspond to one of our GCM basis functions $\Phi_{II}^{JM\pi}(R)$ with R fixed at the values 3.5 fm for the positive-parity states and 5.0 fm for the negative-parity ones. A slight difference with $\Phi_{II}^{JM\pi}$ arises from the fact that the ${}^{14}\text{C}$ nucleus is described in the LS coupling scheme. Different interactions are employed for the shell-model states, for the α -cluster states, and for the couplings between them. This choice provides a more realistic energy location of the ground-state band with respect to the $\alpha + {}^{14}\text{C}$ threshold than in our calculation. Sakuda *et al.* do not explicitly discuss the problem of molecular bands. For the positive parity, however, they obtain the same band as Buck *et al.* with large reduced α widths. There is no clear indication for excited bands. For the negative parity, they obtain a strong clustering for the 1_3^- and 3_3^- states in agreement with Table III. In our calculation, however, the 1_1^- , 1_2^- , and 3_1^- states also present a non-negligible clustering. The reduced α widths of these states in Ref. 25 agree qualitatively with ours so that we estimate that the band structure we propose is not in contradiction with the work of Sakuda *et al.* The remaining differences are probably due to the lack of flexibility of their molecular configurations.

The band structure suggested by the GCM calculation is compared in Fig. 4 with experiment. The open dots represent theoretical energy locations from Fig. 1. For the sake of clarity, the 1^- band and the non-natural-parity states belonging to the 1^+ band are not shown. The crosses correspond to selected experimental states; the dashed lines represent our proposal for a band structure,

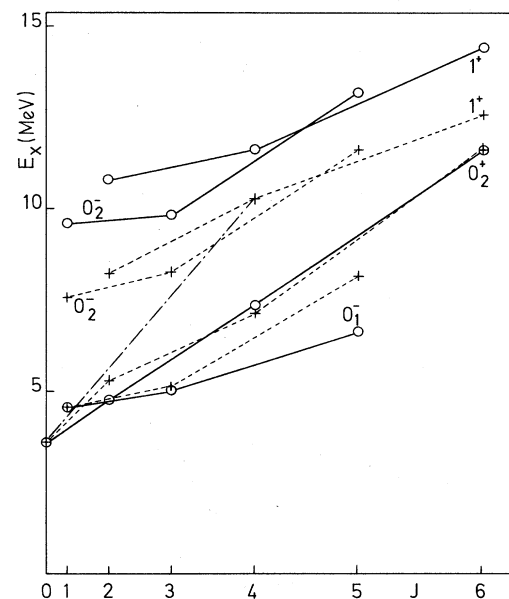


FIG. 4. Comparison between the theoretical (full lines) and the suggested experimental (dashed lines) bands. The molecular band proposed by Gai *et al.* (Ref. 1) is represented by a dash-dotted line.

based on the comparison with the theoretical results. The agreement between the theoretical and experimental 0_2^+ bands is excellent. The small deviation from a pure rotational sequence observed for the experimental 2_3^+ state is probably due to the existence of the 2_2^+ state. The coupling between these states introduces a repulsion between them. This effect cannot be studied in the present model since the description of the 2_2^+ state would require an enlargement of our basis space to other $\alpha + {}^{14}\text{C}^*$ configurations. The existence of the 0_2^+ band can be tested by searching for the missing 8^+ state which is predicted by the model. Its probable location is about 18 MeV.

The agreement between the theoretical and experimental 0_1^- bands is also fair, but the energy of the 5_1^- state is underestimated. This effect is obviously due to too strong a coupling between the two channels since the 5_1^- energy is much better in the single-channel calculation (see Fig. 1). The missing 7^- and 9^- states of the band should also be searched for. Because of the inaccuracy on the 5_1^- energy, predictions about the 7^- and 9^- locations are more difficult, but the 7^- energy should not exceed 13 MeV.

Besides these bands, we propose candidates for three other bands. The 0_2^- band is formed by the 1_3^- , 3_3^- , and 5_2^- experimental states which correspond to excited vibrational states of the $\alpha + {}^{14}\text{C}(0^+)$ configurations. The 1^+ band is composed of the 2_4^+ , 4_3^+ , and 6_2^+ experimental states and has an $\alpha + {}^{14}\text{C}(2^+)$ structure. It would be very interesting to identify the non-natural-parity states of this band. However, the fact that these states are not on a straight line will make their identification rather delicate. Finally, our model suggests that the non-natural-parity 2_1^- state belongs to the same band as the 1_2^- state, with however a less marked clustering. This suggestion seems to be difficult to check experimentally.

The different bands shown in Fig. 4 can be considered as molecular although for some of them the ${}^{14}\text{C}$ cluster is mainly in a 2^+ excited state. The dash-dotted line in Fig. 4 represents the band proposed by Gai *et al.*^{1,2} In the present microscopic interpretation, this band is, in fact, a fortuitous alignment of molecular states belonging to four different molecular bands. The enhancement of transitions between these states is explained in the microscopic model by the important overlap, due to antisymmetrization, between the $\alpha + {}^{14}\text{C}(0^+)$ and $\alpha + {}^{14}\text{C}(2^+)$ configurations.

V. CONCLUSION

Most of the states which exhibit molecular properties are fairly described in the present approach, i.e., with the $\alpha + {}^{14}\text{C}_{\text{g.s.}}$ and one $\alpha + {}^{14}\text{C}^*$ configurations. With respect to the single-channel calculations of Ref. 8, the energies and transition probabilities are in much better agreement with experiment. The fact that among the different excited states of ${}^{14}\text{C}$ located above 6 MeV, the 2^+ (7.01 MeV) state plays the major role, is a consequence of the Pauli principle. The $\alpha + {}^{14}\text{C}(2^+)$ configuration is the most strongly coupled with the $\alpha + {}^{14}\text{C}_{\text{g.s.}}$ one. The introduction of other configurations should improve the quantitative agreement with experiment and allow a description of missing states like the 2_2^+ or 3_2^- states. However, the treatment of the $\alpha + {}^{14}\text{C}(1^-)$ and $\alpha + {}^{14}\text{C}(3^-)$ configurations would be extremely difficult because of the large number of Slater determinants involved. Moreover, if the energies of the ${}^{14}\text{C}$ excited states are not well reproduced by the interaction, the results will be meaningless.¹⁵ The influence of these additional channels might be easier to study in simpler models like the extended cluster model of Ref. 7.

APPENDIX

As effective interaction, we take effective central and spin-orbit forces and the exact Coulomb interaction. The nuclear part of the interaction is parametrized as¹⁷

$$V = \sum_{i=1}^N V_i (1 - m_i + m_i P_M) \exp(-r^2/\mu_i^2) - 2S_0 v^{-5} \hbar^{-2} \mathbf{r} \times \mathbf{p} \cdot \mathbf{s} \exp(-r^2/v^2),$$

where \mathbf{r} , \mathbf{p} , and \mathbf{s} are, respectively, the relative coordinate, relative momentum, and total spin of the two nucleons, P_M is the Majorana exchange operator, and N , V_i , m_i , μ_i , S_0 , and v are parameters. The parameters N , V_i , and m_i are taken from standard effective central forces like the Volkov forces.¹⁹ To reduce the number of parameters, the zero-range approximation is performed for the spin-orbit part of the interaction which is then entirely defined with the strength parameter S_0 .

The energies of the 0^+ and 2^+ ${}^{14}\text{C}$ states are then given by

$$E(0^+) = \frac{59}{4} \hbar\omega + \sum_i V_i \gamma_i^{3/2} \left[\frac{1}{12} (437 + 470\gamma_i + 185\gamma_i^2) - \frac{274}{3} \gamma_i m_i \right] + \frac{34}{3} \frac{e^2}{b} \left[\frac{2}{\pi} \right]^{1/2} - S_0 v^{-5} \gamma_0^{5/2} \frac{10}{3} (5 + 3\gamma_0),$$

$$E(2^+) = \frac{59}{4} \hbar\omega + \sum_i V_i \gamma_i^{3/2} \left[\frac{1}{12} (436 + 472\gamma_i + 184\gamma_i^2) - \frac{272}{3} \gamma_i m_i \right] + \frac{679}{60} \frac{e^2}{b} \left[\frac{2}{\pi} \right]^{1/2} - S_0 v^{-5} \gamma_0^{5/2} \frac{1}{6} (29 + 15\gamma_0),$$

where $\omega = \hbar/m_N b^2$ (m_N being the nucleon mass), $\gamma_i = \mu_i^2/\mu_i^2 + 2b^2$, and $\gamma_0 = v^2/v^2 + 2b^2$

¹M. Gai, M. Rusev, A. C. Hayes, J. F. Ennis, R. Keddy, E. C. Schloemer, S. M. Sterbenz, and D. A. Bromley, Phys. Rev. Lett. **50**, 239 (1983).

²Y. Alhassid, M. Gai, and G. F. Bertsch, Phys. Rev. Lett. **49**,

1482 (1982).

³B. Buck, C. B. Dover, and J. P. Vary, Phys. Rev. C **11**, 1803 (1975).

⁴Y. Suzuki, Prog. Theor. Phys. **55**, 1751 (1976).

- ⁵Y. Fujiwara, H. Horiuchi, K. Ikeda, M. Kamimura, K. Kato, Y. Suzuki, and E. Uegaki, *Prog. Theor. Phys. Suppl.* **68**, 29 (1980).
- ⁶P. Descouvemont and D. Baye, *Phys. Lett.* **127B**, 286 (1983).
- ⁷R. A. Baldock, B. Buck, and J. A. Rubio, *Nucl. Phys.* **A426**, 222 (1984).
- ⁸D. Baye and P. Descouvemont, *Phys. Lett.* **146B**, 285 (1984).
- ⁹H. Horiuchi, *Prog. Theor. Phys. Suppl.* **62**, 90 (1977); Y. C. Tang, in *Topics in Nuclear Physics II*, Lecture Notes in Physics, Vol. 145 (Springer, Berlin, 1981), p. 572.
- ¹⁰D. Baye, P.-H. Heenen, and M. Libert-Heinemann, *Nucl. Phys.* **A291**, 230 (1977).
- ¹¹D. Baye and P. Descouvemont, *Nucl. Phys.* **A407**, 77 (1983).
- ¹²H. J. Assenbaum, K. Langanke, and A. Weiguny, *Z. Phys. A* **318**, 35 (1984).
- ¹³S. Saito, *Prog. Theor. Phys. Suppl.* **62**, 11 (1977).
- ¹⁴M. Libert-Heinemann, D. Baye, and P.-H. Heenen, *Nucl. Phys.* **A339**, 429 (1980).
- ¹⁵D. Baye, P.-H. Heenen, and M. Libert-Heinemann, *Nucl. Phys.* **A308**, 229 (1978).
- ¹⁶F. Ajzenberg-Selove, *Nucl. Phys.* **A360**, 1 (1981).
- ¹⁷D. Baye and N. Pecher, *Bull. Cl. Sc. Acad. R. Belg.* **67**, 835 (1981).
- ¹⁸D. Baye and P. Descouvemont, *Nucl. Phys.* **A419**, 397 (1984).
- ¹⁹A. B. Volkov, *Nucl. Phys.* **74**, 33 (1965).
- ²⁰F. Ajzenberg-Selove, *Nucl. Phys.* **A392**, 1 (1983).
- ²¹A. Bohr and B. R. Mottelson, *Nuclear Structure* (Benjamin, Massachusetts, 1975), Vol. 2.
- ²²B. Buck, H. Friedrich, and A. A. Pilt, *Nucl. Phys.* **A290**, 205 (1977).
- ²³A. Cunsolo, A. Foti, G. Immè, G. Pappalardo, G. Raciti, and N. Saunier, *Phys. Rev. C* **24**, 476 (1981).
- ²⁴P. Descouvemont, D. Baye, and P.-H. Heenen, *Nucl. Phys.* **A430**, 426 (1984).
- ²⁵T. Sakuda, *Prog. Theor. Phys.* **57**, 855 (1977); T. Sakuda, S. Nagata, and F. Nemoto, *ibid.* **59**, 1543 (1978); T. Sakuda, S. Nagata, and F. Nemoto, *Prog. Theor. Phys. Suppl.* **65**, 111 (1979).
- ²⁶G. L. Morgan, D. R. Tilley, G. E. Mitchell, R. A. Hilko, and N. R. Roberson, *Nucl. Phys.* **A148**, 480 (1970).
- ²⁷D. Baye, Thèse d'Agrégation, Université Libre de Bruxelles, 1983 (unpublished).
- ²⁸R. D. Lawson, F. J. D. Serduke, and H. T. Fortune, *Phys. Rev. C* **14**, 1245 (1976).